Spectrochimica Acta Part A: Molecular and Biomolecular Spectroscopy 206 (2019) 295–301

Contents lists available at ScienceDirect

Spectrochimica Acta Part A: Molecular and Biomolecular Spectroscopy

journal homepage: www.elsevier.com/locate/saa

Ultra-fast zinc ion detection in living cells and zebrafish by a light-up fluorescent probe

Zhengliang Lu *, Yanan Lu, Wenlong Fan, Chunhua Fan *, Yanan Li

School of Chemistry and Chemical Engineering, University of Jinan, Jinan 250022, China

ARTICLE INFO

Article history:
Received 5 May 2018
Received in revised form 13 August 2018
Accepted 14 August 2018
Available online 16 August 2018

Keywords:
Light-up
Fluorescent probe
Zinc
Living cells
Bioimaging

ABSTRACT

As the second most abundant transition metal after iron in biological systems, Zn^{2+} takes part in various fundamental life processes such as cellular metabolism and apoptosis, neurotransmission. Thus, the development of analytical methods for fast detection of Zn^{2+} in biology and medicine has been attracting much attention but still remains a huge challenge. In this report, we develop a novel Zn^{2+}-specific light-up fluorescent probe based on intramolecular charge transfer combined with chelation enhanced fluorescence induced by structural transformation. Addition of Zn^{2+} in vitro can induce a remarkable color change from colorless to green and a strong fluorescence enhancement with a red shift of 43 nm. Moreover, the probe shows an extremely low detection limit of 13 nM and ultra-fast response time of less than 1 s. The Zn^{2+} sensing mechanism was fully supported by TDDFT calculations as well as HRMS and ^1H NMR titrations. The recognition of Zn^{2+} in living Hela cells as well as the MTT assay demonstrate that the probe can rapidly light-up detect Zn^{2+} in vivo with low cytotoxicity and good cell-permeability. Furthermore, the probe can also be successfully applied to bioimaging Zn^{2+} in living zebrafish.

1. Introduction

As the second most abundant micronutrient transition metal behind iron in biology, it is well known for decades that Zn^{2+} plays multifunctional roles in fundamental biological processes, such as gene transcription and expression, neural signal transmission, cell division and proliferation, immune activity [1,2]. Due to zinc being an important structural cofactor and catalytic center of hundreds of zinc proteins and regulators of enzymes, deficiency of zinc ion might be associated with severe risks of physical growth retardation and neurological disorders such as cerebral ischemia and Alzheimer's disease, amyotrophic lateral sclerosis, Parkinson's disease and hypoxia-ischemia [3]. However, an excess zinc level might contribute superficial skin diseases, diabetes, and brain diseases. Furthermore, trace amount of free Zn^{2+} might significantly perturb zinc homeostasis in biology due to its strong affinity [4,5]. The clinic studies confirmed that zinc may also prevent esophageal cancer cells proliferation through Orai1-mediated intracellular Ca^{2+} oscillated ions [6]. Therefore, there is an increasing demand for effective and portable detection methods to spatiotemporally monitor biological zinc ion fluctuation.

Compared with conventional methods for Zn^{2+} detection including potentiometry, enzymatic assay, surface acoustic wave spectroscopy, mass spectrometry and electrochemistry, fluorescence spectroscopy is a particularly preferable tool for detection of interesting analytes due to its operational simplicity, high sensitivity and selectivity, and ease of observation [7–10]. Thus, numerous Zn^{2+}-specific fluorescent chemosensors have been reported based on various fluorescent dyes as signal groups, such as 3-hydroxychromone [11], peptide [12], diazafluorene [13], coumarin [14], naphthalene [15,16], quinoline [17,18], boron-dipyrromethene [19], fluorescein [20] and others [21,22], which are bearing chelating moieties as Zn^{2+}-sensing groups such as piperidine/pyridine tripods. Binding of Zn^{2+} with those sensor molecules can significantly regulate electron processes including photo-induced electron transfer (PET), intramolecular charge transfer (ICT) [23], excited-state intramolecular proton (ESIPT) [24,25] or chelation enhanced fluorescence (CHEF) leading to dramatic spectra or color changes.

It is to be noted that most probes in literatures demonstrated excellent fluorescence and/or color changes with short-wavelength light excitation and/or emission probably inducing photobleaching, cellular auto fluorescence, and photo-damage to tissues or organelles. To overcome this drawback, several groups reported their contributions with excitation of long wavelength light [26–31]. For example, Kim's group reported a Golgi-localized two-photon (TP) probe for imaging zinc ions based on the TP fluorophore 6-(benzo[*d*]thiazol-20-yl)-2-(*N*,*N*-dimethylamino) naphthalene in EtOH/MOPS buffer (v:v, 1/1) on excitation at 750 nm [32]. Zhao's group developed a three-photon probe for the imaging of exogenous Zn^{2+} in live cells with varying emission under excitation at 1200 nm [30]. Recently, Tian's group demonstrated a two-photon ratiometric fluorescent probe for bioimaging Zn^{2+} in hippocampal tissue and zebrafish in

* Corresponding authors.
E-mail addresses: zhengliang.lu@yahoo.com (Z. Lu), chm_fanch@ujn.edu.cn (C. Fan).

https://doi.org/10.1016/j.saa.2018.08.025
1386-1425/

EtOH/HEPES buffer (v:v, 1/1) upon excitation at 800 nm, which suffered the interference of Cu^{2+} [33]. Meng's group reported a mitochondria-targeted ratiometric two-photon fluorescent probe for biological Zn^{2+}, in which Cd^{2+} slightly interfere the detection [34]. Unfortunately, these TP and OP fluorescent probes for Zn^{2+} detection more or less showed at least one of drawbacks including long response time, or high limits of detection besides the interference of Cu^{2+}, Cd^{2+} or Fe^{3+} due to their similar properties [35–37].

Our former investigations showed that the cyano electron-withdrawing group can modulate the electron transfer process which finally induce changes of the absorption/emission spectra [38–40]. Therefore, we envision that introduction of a cyano group could extremely lower the HOMO and LUMO level of probe-analyte complex other than the free probe, which probably induced a red shift. Encouraged by these excellent studies and considering those limitations in mind, herein we describe a simple fluorescent probe for ultrafast detection of Zn^{2+} with high selectivity and sensitivity designed by coordination-induced structural transformation. The probe was easily prepared with good yield via one-step condensation of 3′-formyl-4′-hydroxy-[1,1′-biphenyl]-4 carbonitrile and 2-aminobenzohydrazide under mild conditions. As expected, complexation with Zn^{2+} can switch on a large fluorescence enhancement of **P-OH** in 1 s, showing extremely low detection limit and fast response time. The MTT assay and recognition of Zn^{2+} in living Hela cells showed low cytotoxicity and good cell-permeability of the probe. Furthermore, **P-OH** could be successfully applied to bioimaging Zn^{2+} in living zebrafish.

2. Experimental

2.1. Reagents and Chemicals

All chemical reagents were obtained commercially from Aladdin, J&K or Sinopharm Chemical Reagent Co. and used as received without further purification unless otherwise stated. All solvents were purified using standard methods. 3′-formyl-4′-hydroxy-[1,1′-biphenyl]-4 carbonitrile (**1**) and 2-aminobenzohydrazide (**2**) were synthesized according to revising procedures following literatures [38].

2.2. Instruments and Measurements

Ultrapure water was purified from Millipore. ^{1}H NMR and ^{13}C NMR spectra were carried out on a Bruker Advance DRX 400 spectrometer at 400 MHz/100 MHz with TMS as an internal reference. Mass spectra (ESI) were conducted on Bruker Waters-Q-TOF-Premier spectrometer or a Shimadzu LCMS-IT-TOF spectrometer. UV–Vis and Fluorescence spectra were recorded on a TU-1901 spectrophotometer and a Hitachi F-7000 luminescence spectrometer with xenon lamp, respectively. The pH value was measured using a Metrohm 808 Titrando pH meter. Twice-distilled water used throughout all experiments was purified by a Milli-Q system (Milipore, USA). The fluorescence images of cells and zebrafish were taken using a confocal laser scanning microscope (Leica, TCS SP5, Germany) with an objective lens (×40).

2.3. Synthesis of P-OH

Under N_2 atmosphere, 2-aminobenzohydrazide (1 mmol, 0.15 g) and 3′-formyl-4′-hydroxy-[1,1′-biphenyl]-4 carbonitrile (1 mmol,0.20 g) were mixed in 20 mL of ethanol. The mixture was stirred for 6 h under refluxing. After the reaction finished, the solvent was removed under reduced pressure. The crude product was recrystallized from ethanol to give 200 mg of the pure title compound as a yellow solid in 60% yield. ^{1}H NMR (400 MHz, DMSO d_6) δ ppm: 12.05 (s, 1H), 11.83 (s, 1H), 8.65 (s, 1H), 7.95 (d, J = 2.0 Hz, 1H), 7.90 (s, 4H), 7.72 (dd, J = 8.4, 2.2 Hz, 1H), 7.61 (d, J = 7.7 Hz, 1H), 7.26–7.19 (m, 1H), 7.07 (d, J = 8.6 Hz, 1H), 6.77 (d, J = 8.2 Hz, 1H), 6.62–6.56 (m, 1H), 6.51 (s, 2H). ^{13}C NMR (100 MHz, DMSO d_6) δ ppm: 165.6, 158.6, 150.8, 147.5, 144.3, 133.2, 133.1, 130.1, 129.7, 128.8, 128.6, 127.3, 119.8, 119.5, 117.7, 117.0, 115.1, 112.8, 109.7. HRMS (ESI) calc. for $[C_{20}H_{17}N_3O_2\text{-}H]^-$, 355.11950; found, 355.11991.

2.4. Synthesis of *Ref*

The compound was prepared using benzaldehyde following the same procedure as **P-OH** in 73% yield. ^{1}H NMR (400 MHz, DMSO d_6) δ ppm: 11.62 (s, 1H), 8.40 (s, 1H), 7.71 (d, J = 7.1 Hz, 2H), 7.63–7.55 (m, 1H), 7.45 (dt, J = 12.4, 6.8 Hz, 3H), 7.26–7.16 (m, 1H), 6.82–6.73 (m, 1H), 6.64–6.55 (m, 1H), 6.39 (s, 2H).

2.5. General Procedure for Spectra Measurement

A stock solution containing 1.0 mM of **P-OH** was prepared in THF for all fluorescence measurements below. Stock solutions of analytes (Zn^{2+}, Ni^{2+}, Mg^{2+}, Al^{3+}, Ag^{+}, Ba^{2+}, Ca^{2+}, Cr^{3+}, Cu^{2+}, Fe^{3+}, Hg^{2+}, K^{+}, Li^{+}, Mn^{2+}, Na^{+}, Pb^{2+}, Cd^{2+} as their chloride, perchlorate, or nitrate) were prepared in distilled deionized water, respectively. A typical test solution was prepared by mixing 0.01 mL of probe **P-OH** (1.0 mM) and 0.390 mL of THF, appropriate aliquot of each analyte stock solution which was diluted to 1 mL with PBS buffer (20 mM, pH 7.4). The resulting solutions were mixed well for 10 min before recording the fluorescence and UV absorption spectra. The corresponding fluorescence spectrum was performed under excitation at 360 nm.

2.6. Cell Culture and Fluorescence Imaging

HeLa cells were incubated in Dulbeco's Modified Eagle Medium (DMEM) supplemented with 10% fetal bovine serum (10%), penicillin (100 U/mL), and streptomycin (100 U/mL) at 37 °C in a 95% humidity atmosphere containing 5% CO_2. After washing with Dulbecco's phosphate-buffered saline (DPBS) twice, HeLa cells were incubated for 12 h in a flatbottom 96-well plate in 100 μL of culture medium and incubated in 5% CO_2 at 37 °C. The cytotoxic effect of **P-OH** was determined by MTT assays after the 24 h incubation of the cells with the probe at different concentrations (0.0, 2.0, 5.0, 10.0, 15.0, and 20.0 μM).

2.7. In Vivo Imaging of Zebrafish

2-day old zebrafish were provided by the Eze-Rinka Biotechnology Co., Ltd. For fluorescence, the zebrafish were incubated with the aqueous solution of Zn^{2+} (100 μM) for 10 min, and then imaged after PBS buffer. In the experimental group, the zebrafish pretreated with Zn^{2+} (100 μM) for 10 min were incubated with **P-OH** (5 μM). The images of zebrafish were obtained on a confocal microscope with an excitation at 405 nm and the collection wavelength range from 500 to 550 nm.

3. Results and Discussion

3.1. Design and Synthesis of P-OH

Rational combination of donor and acceptor moieties has been extensively used to construct various fluorescent probes specifically for metal ion detection due to their high binding ability [41]. **P-OH** was successfully synthesized by a one-step condensation of 2-aminobenzohydrazide and 3′-formyl-4′-hydroxy-[1,1′-biphenyl]-4 carbonitrile in good yield (See Scheme 1). All compounds were fully characterized by ^{1}H NMR, ^{13}C NMR and ESI-MS analysis (SI, Figs. S1–S4).

With the probe in hand, we initially investigated whether **P-OH** was suitable for Zn^{2+} detection by UV–visible spectra. As shown in Fig. 1, the spectrum of free **P-OH** (10 μM) exhibited two intense absorption bands at 297 and 357 nm in THF aqueous solution (v/v, 4:6, pH 7.4, HEPES 20 mM). Addition of Zn^{2+} resulted in the 5 nm red shift of the band at 297 nm and the disappearance of the band at 357 nm. Simultaneously, a new small band at around 400 nm formed, which was attributed to

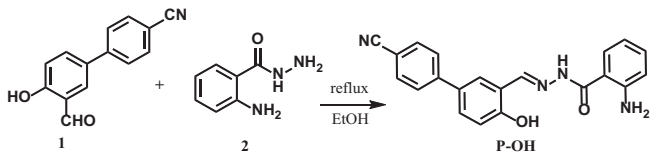

Scheme 1. Synthesis of probe P-OH.

ligand-metal charge transfer. Meanwhile, a fast color change from colorless to green in few seconds upon exposure to UV light (365 nm) was observed. The bands slightly increased upon gradual addition of Zn^{2+} (Fig. S5). As shown in Fig. S6, the initial interfering experiments of **P-OH** demonstrated its high selectivity toward Zn^{2+} over other common metal ions except Cd^{2+}. These remarkable changes indicate **P-OH** could serve as a potential probe for fast Zn^{2+} detection.

In order to investigate the sensitivity of **P-OH** toward Zn^{2+}, the fluorescence titrations of **P-OH** were performed by 30 min incubation with Zn^{2+} in THF aqueous solution (v/v, 4:6, pH 7.4, HEPES 20 mM). As can be seen from Fig. 2a, **P-OH** showed a weak fluorescence emission at 467 nm without Zn^{2+} upon excitation at 360 nm, which could be assigned to a PET process from imino group to biphenol part. This effect probably arose from a less efficient coplanarity limited by intramolecular hydrogen bonding with hydrogen atom of the hydroxyl group in the absence of metal ions. Addition of Zn^{2+} to the solution of **P-OH** immediately moved a fluorescent emission from 467 nm to 510 nm. The large red shift of 43 nm was clearly attributed to the chelation between **P-OH** and Zn^{2+}, which led to the combination of strong ICT and CHEF processes. The fluorescence at 510 nm enhanced with gradual addition of Zn^{2+} and reached the maximum on adding 6 equiv. of Zn^{2+}, a 5-fold increase as compared with that of free probe. This emission enhancement as well as the large red shift suggested that **P-OH** is an excellent turn-on fluorescent chemosensor for Zn^{2+}. Furthermore, a good linearity was found between the fluorescence emission intensity of **P-OH** at 510 nm with increasing concentration of Zn^{2+} ranging from 0 to 30 μM with a R^2 value of 0.994, as shown in Fig. 2b. With respect to these data, the limit of detection (LOD) was calculated to be 13 nM based on $3\sigma/m$, where σ is the standard deviation of the blank measurements, and m is the slope of the intensity versus sample concentration plot. This LOD is comparable with other Zn^{2+}

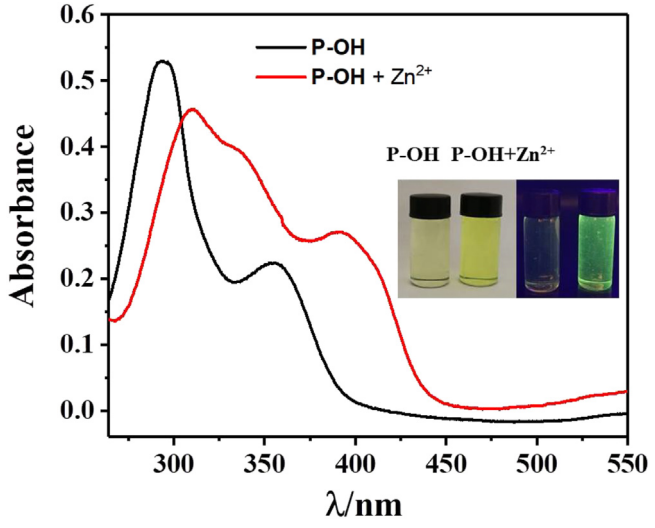

Fig. 1. Absorption spectral changes of **P-OH** (10 μM) in the absence and presence of Zn^{2+} (10 equiv.) in THF aqueous solution (4:6, v/v, HEPES 20 mM, pH 7.4). The measurements were performed after the addition of Zn^{2+} for 30 min. Inset: graphs under natural light or UV light.

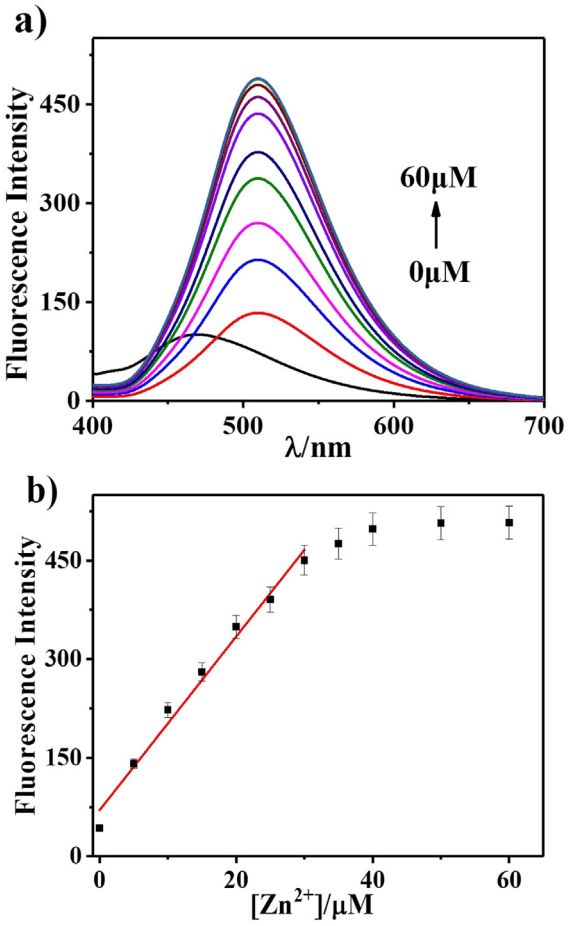

Fig. 2. (a) Fluorescence emission spectra of **P-OH** (10 μM) in the presence of increasing concentrations of Zn^{2+} (0, 5, 10, 15, 20, 25, 30, 35, 40, 50, 60 μM) in THF aqueous solution (4:6, v/v, HEPES 20 mM, pH 7.4). (b) Calibration curve of the fluorescence intensities (I_{510}) versus the concentration of Zn^{2+}. λ_{ex} = 360 nm. The measurements were performed after the addition of Zn^{2+} for 10 min.

fluorescent probes reported (Table S1) and much lower than the Zn^{2+} total concentrations of 200–300 μM in human cells [42]. In order to determine the binding stoichiometry between **P-OH** and Zn^{2+}, a Job's plot on the maximum emission intensity at 510 nm toward the mole ratio of **P-OH** and Zn^{2+} was analyzed (shown in Fig. S7). The maximum emission intensity observed at a mole fraction of 0.3 supported a 1:2 binding stoichiometry between Zn^{2+} and **P-OH**. Based on this, the binding constant of 2.48×10^4 M^{-1} was calculated by Benesi-Hilderbrand equation (Fig. S8).

3.2. Selectivity of P-OH Toward Zn^{2+}

To investigate the affinity of the probe to metal ions, competition experiments of **P-OH** (10 μM) were performed with various metal ions (200 μM) in THF buffer solution (4:6, v/v, HEPES 20 mM, pH 7.4) and the respective fluorescence intensities were displayed in Fig. 3. Apparently, Zn^{2+} induced a dramatic fluorescence enhancement and color change although Cd^{2+} led to a slightly fluorescent change. As expected, no considerable fluorescent intensity changes at 510 nm could be detected in the presence of other common metal ions such as Ni^{2+}, Mg^{2+}, Al^{3+}, Ag^{+}, Ba^{2+}, Ca^{2+}, Cr^{3+}, Cu^{2+}, Fe^{3+}, Hg^{2+}, K^{+}, Li^{+}, Mn^{2+}, Na^{+}, Pb^{2+}, and Cd^{2+} over a period of 30 min. These results evidenced that **P-OH** binding Zn^{2+} is not obviously interfered by other coexisting metal ion or anions, which indicates that **P-OH** could be a two-output fluorescent probe for Zn^{2+} with high specificity. As shown in Fig. S9, the reversibility of **P-OH** binding Zn^{2+} was evidenced on addition of a

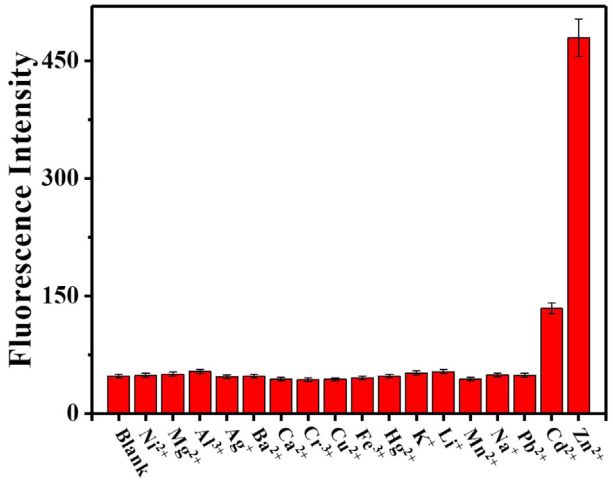

Fig. 3. Fluorescence responses of the probe **P-OH** (10 μM) upon addition of different carious relevant species (10 equiv.) in THF aqueous solution (4:6, v/v, HEPES 20 mM, pH 7.4). The measurements were performed after the addition of Zn^{2+} for 30 min. $\lambda_{ex} = 360$ nm.

strong chelating agent EDTA. EDTA induced a significant decrease in emission intensity. The fluorescence intensity of probe gradually descended and reached to that of free probe with the addition of 2 equiv. of EDTA, which testifying the strong binding affinity of **P-OH** for Zn^{2+} in 40% THF aqueous solution (4/6, v:v, HEPES, 20 mM, pH 7.4).

As a significant parameter as chemosensors, response time was investigated. The kinetic profile of the reaction of **P-OH** and Zn^{2+} at room temperature was showed in Fig. S10. The fluorescence emission of **P-OH** reached equilibrium within 1 s after injection of Zn^{2+} in THF-buffer. The emission intensity did not show obvious fluorescence change over the subsequent 120 s, confirming the probe-Zn^{2+} complex stable. The fluorescence emission intensities of **P-OH** upon addition of Zn^{2+} at different concentrations (0, 20, 60 μM) showed that the response time is almost concentration-independent. These results demonstrated that our proposed probe would provide a rapid analytical method for Zn^{2+} detection.

3.3. Effect of pH

In extend the application of **P-OH** in biological systems, the influence of pH dependency on fluorescence intensity at 510 nm of **P-OH** in the absence and presence of Zn^{2+} was conducted at various pH values in THF-buffer (4:6, v/v) solution. As shown in Fig. S11, the fluorescence emissions sharply increased when the solution of free **P-OH** was in a more basic environment (pH ˃ 8.5). This is likely because the deprotonation of hydroxyl group was deprotonated at high pH. Furthermore, the structural transformation from amide to imidic acid tautomer promoted by the basic condition also made an important contribution forming a bigger conjugated system, which enhanced the ICT effect on a large scale. In contrast, the fluorescence intensity of probe-Zn^{2+} remarkably increased from pH 2.0 and reached a plateau at pH 4.0 with no obvious change after pH ˃ 4.0. The wide pH range from 4.0 to 8.5 demonstrates that **P-OH** can be used as a fluorescent probe for Zn^{2+} detection under physiological conditions.

3.4. The Proposed Mechanism of P-OH Sensing Zn^{2+}

Light-up fluorescent probes for Zn^{2+} detection are much preferable than light-off ones due to their advantages such as ease of observation. Inspired by our former research results, we envision that a strong electron-deficient group could largely change the electron density distribution of the target compound so that the fluorescence can be switched on or off. Thus, **P-OH** was designed as a potential push-pull system containing a cyano electron-withdrawing group and an amino electron-donating group. The three-atom cage composed of amide, hydroxyl, and imino groups could accommodate Zn^{2+} forming a stable coordination complex. A proposed mechanism for the enhanced fluorescence response of **P-OH** sensing Zn^{2+} was depicted in Scheme S1. The PET process from imino group to biphenol part probably led to very weak emission of **P-OH**. As we designed, only addition of Zn^{2+} can promote and induce the remarkable fluorescence enhancement of **P-OH,** which was reasonably attributed to combination of both ICT and CHEF. This is beneficial from two aspects: 1) Structural transformation from amide to imidic acid tautomer could enlarge the conjugated system along imine and amide parts; and 2) A free rotation was much more inhibited by Zn^{2+} than weak intra-molecular hydrogen bonding. In order to substantiate our rational design, a reference compound **Ref** without cyano and hydroxyl groups was prepared from benzaldehyde following the same procedure as **P-OH**. Due to lack of hydroxyl group in **Ref**, there could not be the preferable three-atom cage to strongly bind Zn^{2+}, which led to the formation of imidic acid tautomer and enlargement of the conjugation. Furthermore, the electron distribution was not changed much with the cyano group. Thus as shown in Fig. S12, no obvious fluorescence changes was observed. Next, HRMS spectra was performed to verify this reaction mechanism. The ESI-MS spectra demonstrated a characteristic molecular ion peak at m/z = 355.11950 [M-H^+] corresponding to the free probe (calcd 355.11991) as shown in Fig. S3. Upon complexation with Zn^{2+} (1 equiv.), an obvious peak at m/z = 419.04822 [M + Zn^{2+}-H^+] in solution of **P-OH** (Fig. S13) corresponds to the probe-Zn^{2+} complex (calcd 419.04865). Most importantly, a prominent peak at m/z = 775.17523 [2 M + Zn^{2+}-H^+] was assigned to the 2probe:Zn^{2+} complex (calcd 775.17597), fully consistent with the 1:2 stoichiometry (Job's plot).

To investigate the mechanism of the probe sensing Zn^{2+} in detail, ^{1}H NMR titrations of the probe were conducted in the absence and presence of Zn^{2+} in DMSO d_6, respectively. As shown in Figs 4a and S1, the chemical shift at δ 12.05 and 11.83 ppm are probably assigned to protons of hydroxyl and amide group of **P-OH**, respectively. In fact, the integration of the peak for amide proton is less than a proton, indicating the existence of enolization from amide. Once Zn^{2+} was added, both amide and hydroxyl protons completely diminished, which evidenced the binding of Zn^{2+} and **P-OH** (Figs. 4b and S14). Furthermore, the binding of Zn^{2+} induced the chemical-shift changes of the para- and ortho proton of hydroxyl group as well as other unobvious changes. Compared with the free probe, the disappearance of the peaks at 11.83 ppm of **P-OH**-Zn^{2+} suggested that amide (–NH-C(═O)–) was transformed into imidic acid tautomer (–(N═C(OH)–). This kind of structural transformation would extremely strengthen and enlarge the conjugated degree along the long bridge between aminobenzene and hydroxyl-benzene moieties no matter in the presence of Zn^{2+}. The ^{1}H NMR spectra of **Ref** in DMSO d_6 was recorded and demonstrates the chemical shifts at 11.62 ppm from amide (Figs. 4c and S4). All these results supported the rationality of the proposed mechanism of **P-OH** sensing Zn^{2+}.

In order to get insight into the abovementioned plausible mechanism, the geometries of **P-OH** and **P-OH**-Zn were optimized by density functional theory (DFT). The singlet excited states for probe **P-OH** and **P-OH**-Zn^{2+} were obtained at the B3LYP/6-31G level using the Gaussian 09 program. As shown in Fig. 5a, the HOMO and LUMO electron densities are mainly distributed to aminobenzene moiety and LUMO electron densities are mainly distributed to hydroxyl-benzene moiety and the bridge including imine and amide moiety. The energy gap between the LUMO and HOMO level in **P-OH** is 2.44 eV. Once **P-OH** coordinated to Zn^{2+}, the HOMO and LUMO in **P-OH**-Zn^{2+} were conversely localized on the whole hydroxyl-benzene moiety with cyano group and aminobenzene one, respectively (Fig. 5b). Apparently, this phenomenon was attributed to the enlargement of conjugated system due to the complexation of the probe and Zn^{2+}. However, there was no obvious electron distribution on the cyano group of free probe due to that the less efficient conjugation. The lower energy gap of 1.8 eV

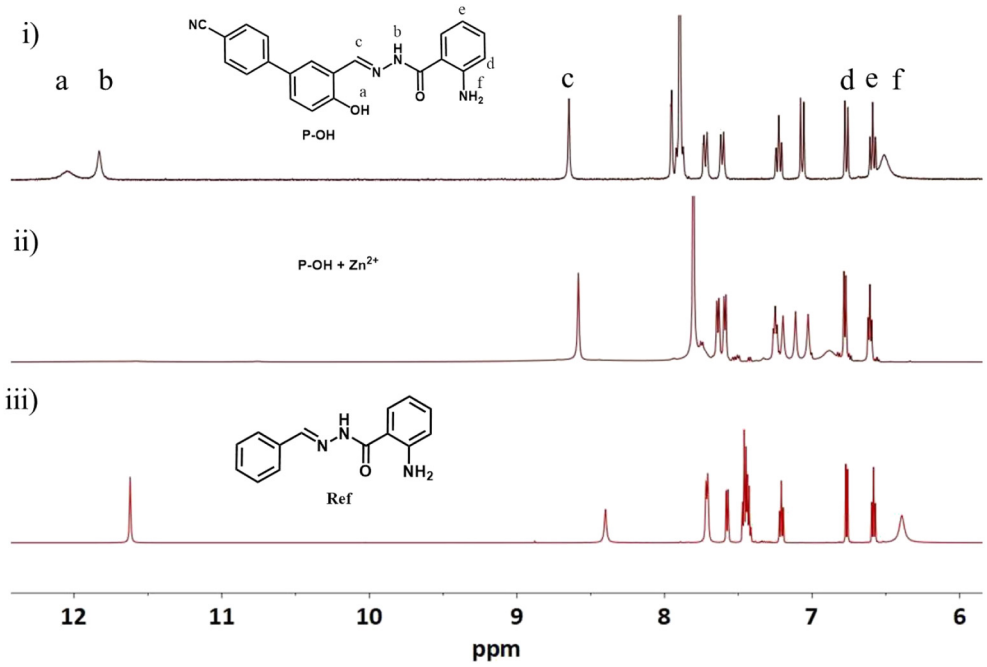

Fig. 4. Partial ^{1}H NMR spectra of (i) **P-OH** in DMSO d_6, (ii) **P-OH**-Zn^{2+} in DMSO d_6, (iii) **Ref** in DMSO d_6.

between the HOMO and LUMO level of 2probe:Zn^{2+} compared with 2.11 eV of probe:Zn^{2+} was in good agreement with the red shift of the experimental absorption fluorescence spectra (Fig. 5c).

3.5. Imaging Zn^{2+} in Living Cells

Based on its good selectivity and sensitivity, first, a standard MTT assay was conducted to assess the cell cytotoxicity of the probe. HeLa cells were incubated with different concentration probe **P-OH** (0, 2, 5, 10, 15, 20 μM) for 24 h. As shown in Fig. S15, even with 15 μM probe, there was no obvious influence on HeLa cells with the cell viability of 90% for an incubation time of as long as 24 h. These results suggested its low cytotoxicity and good biocompatibility to living HeLa cells.

Subsequently, we estimated the practical utility of this probe to visualize hydrazine in living cells with a confocal microscope (Leica, Germany). As shown in Fig. 6a–c, HeLa cells did not emit any obvious intracellular background fluorescence at 405 nm excitation. As expected, we still could not observe the fluorescence emission after HeLa cells were incubated with probe **P-OH** (5 μM) in DMEM for 30 min at 37 °C (Fig. 6d–f). However, in the experimental group, the remarkable green fluorescence was detected when HeLa cells were pretreated with 10 μL of probe **P-OH** (5 μM) for 30 min and then further with Zn^{2+} (100 μM) for another 30 min (Fig. 6g–i). Bright-field images of HeLa cells showed that the cells pretreated with probe retained a good morphology (Fig. 6d, g). This strong fluorescence emission confirmed that this probe is cell-membrane-permeable. These results indicate that probe **P-OH** can detect intracellular Zn^{2+} in living cells.

3.6. Imaging Zn^{2+} in Zebrafish

Based on the prominent fluorescent Zn^{2+}-sensing performance in the living cells, we test the feasibility of bioimaging Zn^{2+} in live Zebrafish with a Leica confocal microscope. First, 2-day-old zebrafish was incubated with 5 μM of the probe for 30 min. As show in Fig. 7a–c, no matter under

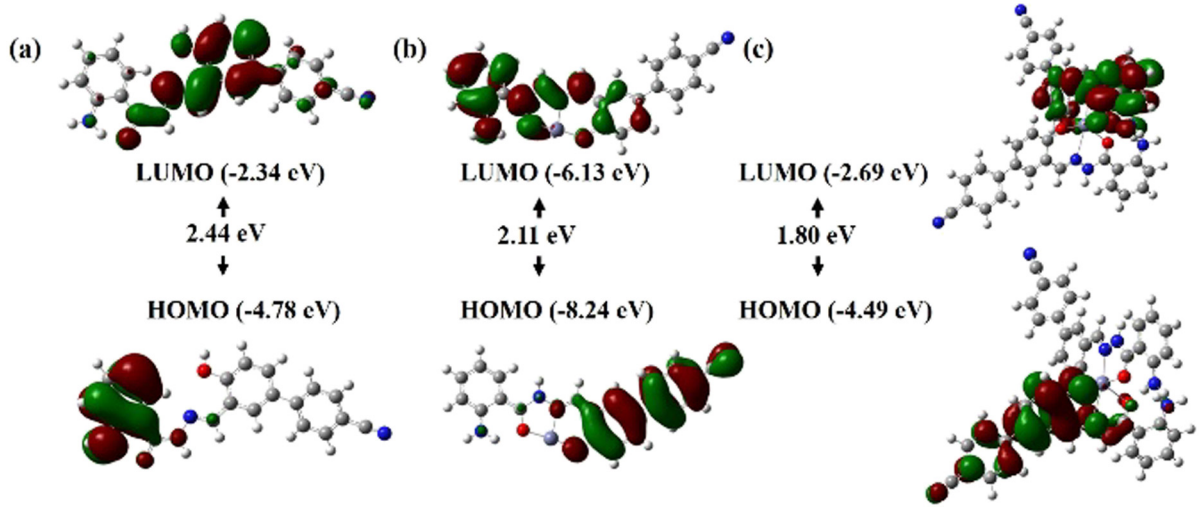

Fig. 5. Optimized structures and frontier molecular orbitals of (a) **P-OH**, (b) **P-OH**:Zn^{2+} and (c) 2 **P-OH**:Zn^{2+} calculations were performed at B3LYP/6-31G level.

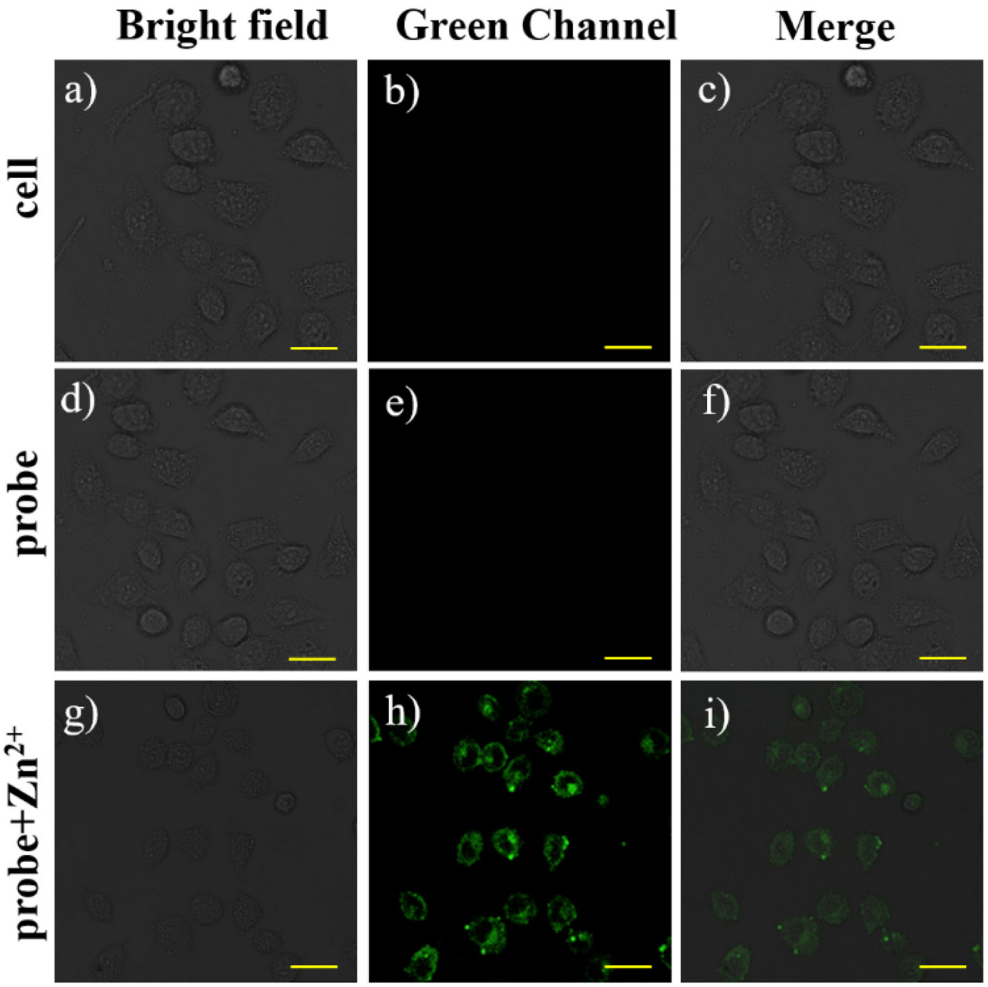

Fig. 6. Confocal fluorescence images of living HeLa cells treated with **P-OH** in the absence and presence of Zn^{2+}. (a) Image of HeLa Cells. (b) Bright field image of (a). (c) Merging of (a) and (b). (d) Image of HeLa cells with **P-OH**. (e) Bright field image of (d). (f) Merging of (d) and (e). (g) Image of HeLa cells with **P-OH** and Zn^{2+}. (h) Bright field image of (g). (i) Merging of (g) and (h). $\lambda_{ex} = 405$ nm; green channel: $\lambda_{em} = 500–550$ nm. Scale bar: 20 μm. (For interpretation of the references to color in this figure legend, the reader is referred to the web version of this article.)

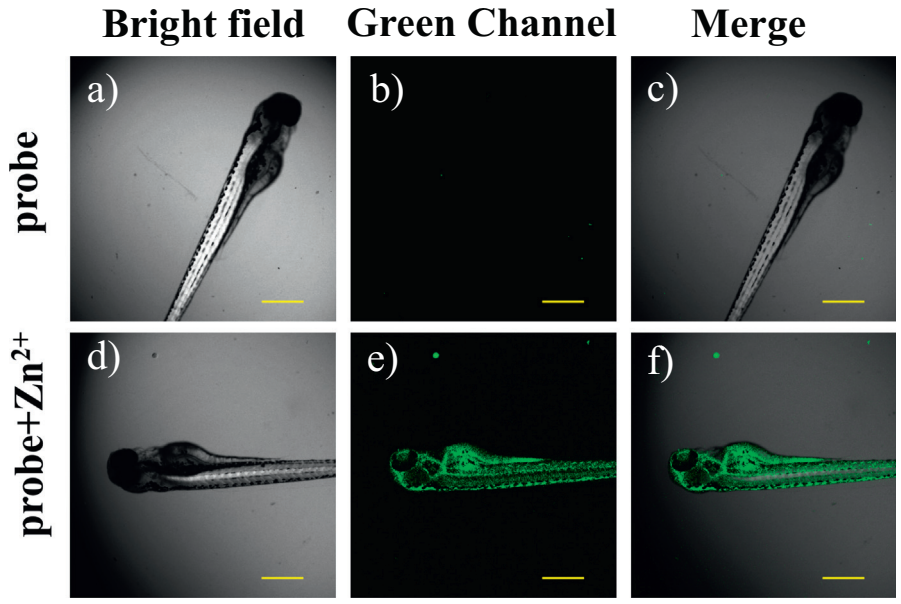

Fig. 7. Confocal fluorescence images of living zebrafish treated with **P-OH** with or without Zn^{2+}. (a) Images of zebrafish. (b) Bright field image of (a). (c) Merging of (a) and (b). (d) Image of zebrafish with **P-OH**. (e) Bright field image of (d). (f) Merging of (d) and (e). $\lambda_{ex} = 405$ nm; green channel: $\lambda_{em} = 500–550$ nm; scale bar: 20 μm. (For interpretation of the references to color in this figure legend, the reader is referred to the web version of this article.)

bright or fluorescent field, the live zebrafish did not emit any detectable fluorescence. In the second group, the zebrafish was treated with probe **P-OH** (5 μM) for 30 min and then followed with an incubation of Zn^{2+} (100 μM) for another 30 min. After washed three times with HEPES, the zebrafish emits strong green fluorescence (Fig. 7d–f). These results suggested that **P-OH** could be used for bioimaging Zn^{2+} in vivo.

4. Conclusion

In summary, we have successfully developed a simple light-up fluorescent probe for Zn^{2+} with high selectivity and sensitivity. The probe exhibited a remarkable color change from colorless to green and a strong fluorescence enhancement upon addition of Zn^{2+} with fast response time of less than 1 s under physiological conditions. Theoretical calculations as well as HRMS and ^1H NMR titrations of the probe with Zn^{2+} were good agreement with this rational design and the recognition mechanism. The probe can detect Zn^{2+} in living HeLa cells with excellent biocompatibility and low cell cytotoxicity. Moreover, the probe has been successfully used to bioimage Zn^{2+} in living zebrafish models.

Acknowledgments

We thank for the supporting from Natural Science Foundation of China (grant no. 21101074), Shandong Provincial Natural Science Foundation of China (grant no. ZR2013BQ009 and ZR2016BL17), the Doctor's Foundation of University of Jinan (grant no. XBS1320).

Appendix A. Supplementary Data

NMR spectra of the compounds, MS and chromatograms of the reaction systems, supplementary fluorescent spectra, cytotoxicity assay. Supplementary data to this article can be found online at https://doi.org/10.1016/j.saa.2018.08.025.

References

[1] J.M. Berg, Y. Shi, The galvanization of biology: a growing appreciation for the roles of zinc, Science 271 (1996) 1081–1085.
[2] C.J. Frederickson, J.-Y. Koh, A.I. Bush, The neurobiology of zinc in health and disease, Nat. Rev. Neurosci. 6 (2005) 449–462.
[3] A.I. Bush, W.H. Pettingell, G. Multhaup, M. d Paradis, J.P. Vonsattel, J.F. Gusella, K. Beyreuther, C.L. Masters, R.E. Tanzi, Rapid induction of Alzheimer A beta amyloid formation by zinc, Science 265 (1994) 1464–1467.
[4] A.M. Hessels, M. Merkx, Genetically-encoded FRET-based sensors for monitoring Zn^{2+} in living cells, Metallomics 7 (2015) 258–266.
[5] J.L. Vinkenborg, T.J. Nicolson, E.A. Bellomo, M.S. Koay, G.A. Rutter, M. Merkx, Genetically encoded FRET sensors to monitor intracellular Zn^{2+} homeostasis, Nat. Methods 6 (2009) 737–740.
[6] S. Choi, C. Cui, Z. Pan, S. Choi, C. Cui, Y. Luo, S.-H. Kim, J. Ma, Z. Pan, C. Cui, L.-W. Fu, Y. Luo, J.-K. Ko, X. Huo, R.F. Souza, J. Ma, I. Korichneva, Selective inhibitory effects of zinc on cell proliferation in esophageal squamous cell carcinoma through Orai1, FASEB J. 32 (2018) 404–416.
[7] Z. Xu, J. Yoon, D.R. Spring, Fluorescent chemosensors for Zn^{2+}, Chem. Soc. Rev. 39 (2010) 1996–2006.
[8] J. Li, C. Yin, F. Huo, Development of fluorescent zinc chemosensors based on various fluorophores and their applications in zinc recognition, Dyes Pigments 131 (2016) 100–133.
[9] P. Jiang, Z. Guo, Fluorescent detection of zinc in biological systems: recent development on the design of chemosensors and biosensors, Coord. Chem. Rev. 248 (2004) 205–229.
[10] J. Peng, W. Xu, C.L. Teoh, S. Han, B. Kim, A. Samanta, J.C. Er, L. Wang, L. Yuan, X. Liu, Y.-T. Chang, High-efficiency in vitro and in vivo detection of Zn^{2+} by dye-assembled upconversion nanoparticles, J. Am. Chem. Soc. 137 (2015) 2336–2342.
[11] X. Li, J. Li, X. Dong, X. Gao, D. Zhang, C. Liu, A novel 3-hydroxychromone fluorescence sensor for intracellular Zn^{2+} and its application in the recognition of prostate cancer cells, Sensors Actuators B 245 (2017) 129–136.
[12] G. Donadio, R. Di Martino, R. Oliva, L. Petraccone, P. Del Vecchio, B. Di Luccia, E. Ricca, R. Isticato, A. Di Donato, E. Notomista, A new peptide-based fluorescent probe selective for zinc(II) and copper(II), J. Mater. Chem. B 4 (2016) 6979–6988.
[13] H. Li, S.J. Zhang, C.L. Gong, J.Z. Wang, F. Wang, A turn-on and reversible fluorescence sensor for zinc ion based on 4,5-diazafluorene Schiff base, J. Fluoresc. 26 (2016) 1555–1561.
[14] Z. Xu, X. Liu, J. Pan, D.R. Spring, Coumarin-derived transformable fluorescent sensor for Zn^{2+}, Chem. Commun. 48 (2012) 4764–4766.
[15] J.H. Lee, J.H. Lee, S.H. Jung, T.K. Hyun, M. Feng, J.-Y. Kim, J.-H. Lee, H. Lee, J.S. Kim, C. Kang, K.-Y. Kwon, J.H. Jung, Highly selective fluorescence imaging of zinc distribution in HeLa cells and *Arabidopsis* using a naphthalene-based fluorescent probe, Chem. Commun. 51 (2015) 7463–7465.
[16] Y. Tang, J. Sun, B. Yin, A dual-response fluorescent probe for Zn^{2+} and Al^{3+} detection in aqueous media: pH-dependent selectivity and practical application, Anal. Chim. Acta 942 (2016) 104–111.
[17] M. Akula, P.Z. El-Khoury, A. Nag, A. Bhattacharya, Selective Zn^{2+} sensing using a modified bipyridine complex, RSC Adv. 4 (2014) 25605–25608.
[18] G.J. Park, J.J. Lee, G.R. You, L.T. Nguyen, I. Noh, C. Kim, A dual chemosensor for Zn^{2+} and Co^{2+} in aqueous media and living cells: experimental and theoretical studies, Sensors Actuators B Chem. 223 (2016) 509–519.
[19] J.-R. Lin, C.-J. Chu, P. Venkatesan, S.-P. Wu, Zinc(II) and pyrophosphate selective fluorescence probe and its application to living cell imaging, Sensors Actuators B 207 (2015) 563–570.
[20] D. Li, L. Liu, W.-H. Li, Genetic targeting of a small fluorescent zinc indicator to cell surface for monitoring zinc secretion, ACS Chem. Biol. 10 (2015) 1054–1063.
[21] S.Y. Lee, S.Y. Kim, J.A. Kim, C. Kim, A dual chemosensor: colorimetric detection of Co^{2+} and fluorometric detection of Zn^{2+}, J. Lumin. 179 (2016) 602–609.
[22] Q. Jiang, Z. Guo, Y. Zhao, F. Wang, L. Mao, In vivo fluorescence sensing of the salicylate-induced change of zinc ion concentration in the auditory cortex of rat brain, Analyst 140 (2015) 197–203.
[23] T. Wei, J. Wang, Y. Chen, Y. Han, Combining the PeT and ICT mechanisms into one chemosensor for the highly sensitive and selective detection of zinc, RSC Adv. 5 (2015) 57141–57146.
[24] J.E. Kwon, S. Lee, Y. You, K.-H. Baek, K. Ohkubo, J. Cho, S. Fukuzumi, I. Shin, S.Y. Park, W. Nam, Fluorescent zinc sensor with minimized proton-induced interferences: photophysical mechanism for fluorescence turn-on response and detection of endogenous free zinc ions, Inorg. Chem. 51 (2012) 8760–8774.
[25] Y. Xu, Y. Pang, Zn^{2+}-triggered excited-state intramolecular proton transfer: a sensitive probe with near-infrared emission from bis(benzoxazole) derivative, Dalton Trans. 40 (2011) 1503–1509.
[26] Z. Mao, L. Hu, X. Dong, C. Zhong, B.-F. Liu, Z. Liu, Highly sensitive quinoline-based two-photon fluorescent probe for monitoring intracellular free zinc ions, Anal. Chem. 86 (2014) 6548–6554.
[27] K.P. Divya, S. Sreejith, P. Ashokkumar, K. Yuzhan, Q. Peng, S.K. Maji, Y. Tong, H. Yu, Y. Zhao, P. Ramamurthy, A. Ajayaghosh, A ratiometric fluorescent molecular probe with enhanced two-photon response upon Zn^{2+} binding for in vitro and in vivo bioimaging, Chem. Sci. 5 (2014) 3469–3474.
[28] X. Meng, S. Wang, Y. Li, M. Zhu, Q. Guo, 6-Substituted quinoline-based ratiometric two-photon fluorescent probes for biological Zn^{2+} detection, Chem. Commun. 48 (2012) 4196–4198.
[29] L. Li, J. Feng, Y. Fan, B. Tang, Simultaneous imaging of Zn^{2+} and Cu^{2+} in living cells based on DNAzyme modified gold nanoparticle, Anal. Chem. 87 (2015) 4829–4835.
[30] A.K. Mandal, T. He, S.K. Maji, H. Sun, Y. Zhao, A three-photon probe with dual emission colors for imaging of Zn(II) ions in living cells, Chem. Commun. 50 (2014) 14378–14381.
[31] G. Masanta, C.S. Lim, H.J. Kim, J.H. Han, H.M. Kim, B.R. Cho, A mitochondrial-targeted two-photon probe for zinc ion, J. Am. Chem. Soc. 133 (2011) 5698–5700.
[32] H. Singh, H.W. Lee, C.H. Heo, J.W. Byun, A.R. Sarkar, H.M. Kim, A Golgi-localized two-photon probe for imaging zinc ions, Chem. Commun. 51 (2015) 12099–12102.
[33] W. Li, B. Fang, M. Jin, Y. Tian, Two-photon ratiometric fluorescence probe with enhanced absorption cross section for imaging and biosensing of zinc ions in hippocampal tissue and zebrafish, Anal. Chem. 89 (2017) 2553–2560.
[34] P. Ning, J. Jiang, L. Li, S. Wang, H. Yu, Y. Feng, M. Zhu, B. Zhang, H. Yin, Q. Guo, X. Meng, A mitochondria-targeted ratiometric two-photon fluorescent probe for biological zinc ions detection, Biosens. Bioelectron. 77 (2016) 921–927.
[35] W. Li, X. Tian, B. Huang, H. Li, X. Zhao, S. Gao, J. Zheng, X. Zhang, H. Zhou, Y. Tian, J. Wu, Triphenylamine-based Schiff bases as the high sensitive Al^{3+} or Zn^{2+} fluorescence turn-on probe: mechanism and application in vitro and in vivo, Biosens. Bioelectron. 77 (2016) 530–536.
[36] M.-Y. Jia, Y. Wang, Y. Liu, L.-Y. Niu, L. Feng, BODIPY-based self-assembled nanoparticles as fluorescence turn-on sensor for the selective detection of zinc in human hair, Biosens. Bioelectron. 85 (2016) 515–521.
[37] K. Wechakorn, K. Suksen, P. Piyachaturawat, P. Kongsaeree, Rhodamine-based fluorescent and colorimetric sensor for zinc and its application in bioimaging, Sensors Actuators B Chem. 228 (2016) 270–277.
[38] C. Fan, X. Huang, C.A. Black, X. Shen, J. Qi, Y. Yi, Z. Lu, Y. Nie, G. Sun, A fast-response, fluorescent 'turn-on' chemosensor for selective detection of Cr^{3+}, RSC Adv. 5 (2015) 70302–70308.
[39] W. Fan, X. Huang, X. Shi, Z. Wang, Z. Lu, C. Fan, Q. Bo, A simple fluorescent probe for sensing cysteine over homocysteine and glutathione based on PET, Spectrochim. Acta A 173 (2017) 918–923.
[40] Z. Lu, W. Fan, X. Shi, C.A. Black, C. Fan, F. Wang, A highly specific BODIPY-based fluorescent probe for the detection of nerve-agent simulants, Sensors Actuators B Chem. 255 (2018) 176–182.
[41] A. Senthil Murugan, N. Vidhyalakshmi, U. Ramesh, J. Annaraj, A Schiff's base receptor for red fluorescence live cell imaging of Zn^{2+} ions in zebrafish embryos and naked eye detection of Ni^{2+} ions for bio-analytical applications, J. Mater. Chem. B 5 (2017) 3195–3200.
[42] W. Maret, Analyzing free zinc(II) ion concentrations in cell biology with fluorescent chelating molecules, Metallomics 7 (2015) 202–211.